Journal of Alloys and Compounds 517 (2012) 75–79

Contents lists available at SciVerse ScienceDirect

Journal of Alloys and Compounds

journal homepage: www.elsevier.com/locate/jallcom

# Effects of crystal-alignment and grain shape on the thermoelectric properties of $Bi_{0.5}Sb_{1.5}Te_3$ alloys

Koo-Chul Je[a], Beyungduk Ko[b], Cham Kim[c], Hoyoung Kim[d], Dong-Hwan Kim[d,*]

[a] Department of Physics, College of Liberal Arts and Sciences, Anyang University, Gyeonggi-do 430-714, Republic of Korea
[b] Department of Electronic Physics, Kwangwoon University, Seoul, Republic of Korea
[c] Department of Chemical Engineering, Pohang University of Science and Technology (POSTECH), San 31 Hyoja-dong, Pohang 790-784, Republic of Korea
[d] Daegu Gyeongbuk Institute of Science and Technology, 711-623 Hosan-dong, Dalseo-gu, Daegu 704-230, Republic of Korea

ARTICLE INFO

*Article history:*
Received 23 September 2011
Received in revised form
22 November 2011
Accepted 10 December 2011
Available online 20 December 2011

*Keywords:*
Thermoelectric properties
Alignment
Grain shape
Quantum confinement

ABSTRACT

We investigated the thermoelectric properties of sintered $Bi_{0.5}Sb_{1.5}Te_3$ alloys containing grains for their alignment, sizes and shapes. The figure of merit can be improved as the result of lower resistivity by increasing the alignment, which is realized by using the spark plasma sintering method and a strong magnetic field. In addition, making the grains more spherical can improve the thermoelectric efficiency as a result of carrier quantum confinement and enhancement of the band gap energy.



## 1. Introduction

Binary and ternary compounds of Bi, Sb, Te, and Se prepared using a hot-pressing method [1–3] have been widely investigated for use in thermoelectric devices operating near room temperature because they have highly anisotropic electric and thermal properties with a rhombohedral structure. Powder metallurgy using hot pressing is a powerful tool for fabricating thermoelectric materials because it allows for production in great quantities and control of the microstructure. The prepared materials have grain boundaries and anisotropy due to their alignment. To improve the thermoelectric performance, the thermoelectric properties were extensively investigated by controlling the grain size [4], carrier concentration [5–7] and the crystal alignment [8–10], which can be controlled by using the spark plasma sintering (SPS) method with magnetic fields of different strengths. The alloys prepared by the SPS method have a mixed system containing the polycrystalline and powder phases. We define polycrystalline and powder phases as follows: the polycrystalline phase has grains in which the *c*-axis of the crystallites lies randomly in a plane perpendicular to the growth direction, and the powder has grains in which the *c*-axis is completely randomly oriented. The thermoelectric properties of both materials were theoretically investigated [6,11].

In this study, we investigated the thermal properties of the sintered $Bi_{0.5}Sb_{1.5}Te_3$ alloys. The grains in the prepared alloys have different sizes, irregular shapes and different crystal-alignments. We found that the figure of merit can be improved as the result of lower resistivity from increasing the crystal-alignment and as the result of lower thermal conductivity from making the grains more spherical.

The alloy prepared under pure conditions or a magnetic field using the SPS method has an oriented *c*-axis in a plane perpendicular to the growth direction. The magnetic field introduced a large number of *c*-axes oriented along the plane in the green bodies. The crystal alignment can be controlled by the strength of the magnetic field. The thermoelectric results are presented in Sections 2 and 3.

### 2. Experimental and theory

We obtained powdered $Bi_{0.5}Sb_{1.5}Te_3$ via a powder metallurgy process. The powder was dispersed in anhydrous ethanol and then slip-casted in the presence and absence of a magnetic field. The slip-casted green bodies were sintered with a SPS machine at 500 °C for 2 min in an Ar atmosphere. The experimental details of sample preparation and characterization have been described previously [8–10].

When the Bi, Sb, and Te alloys are sintered by using the SPS method, the alloys have variously oriented grains with various sizes. The grain size and crystal orientation can be determined by the electron backscatter diffraction (EBSD) mappings according to the scanning electron microscopy (SEM) results [8,9]. We defined the polycrystalline phase, in which the *c*-axes of grains are completely aligned along the direction parallel to the pressing direction, and powder phase, in which the *c*-axes

* Corresponding author.
*E-mail addresses:* je_kc@anyang.ac.kr (K.-C. Je), kimdhwan@dgist.ac.kr (D.-H. Kim).

0925-8388/$ – see front matter © 2011 Elsevier B.V. All rights reserved.
doi:10.1016/j.jallcom.2011.12.030

of grains are randomly oriented in the alloys. The sintered alloys are considered to be a mixed system of the polycrystalline phase and the powder phase. The thermal properties of both material structures have been determined from the corresponding single-crystal components, which have anisotropic properties along the cleavage planes (11-direction) and perpendicular to the cleavage planes (33-direction) [11]. The '33' and '11' correspond to the directions parallel and perpendicular to the SPS pressing direction, respectively.

In the model, the alloys have two occupying volume fractions, $V_{Big}$ and $V_{Small}$, which are the total volumes of big and small grains, respectively. The region with the volume $V_{Big}$ consists of the proportions $a_{B,P}$ and $a_{B,W}$ of the polycrystalline and powder phases, respectively, and the other region with volume $V_{Small}$ consists of different proportions of $a_{S,P}$ and $a_{S,W}$ for the polycrystalline and powder phases, respectively. In this case, the conductivity ($\sigma$), thermal conductivity ($\kappa$) and Seebeck coefficient ($\alpha$) are given by

$$\frac{1}{\sigma} = \frac{V_{Big}}{\sigma_B} + \frac{V_{Small}}{\sigma_S} \tag{1}$$

$$\frac{1}{\kappa} = \frac{V_{Big}}{\kappa_B} + \frac{V_{Small}}{\kappa_S} \tag{2}$$

$$\alpha = V_{Big}\,\alpha_B + V_{Small}\,\alpha_S \tag{3}$$

where

$$\frac{1}{\sigma_i} = \frac{a_{i,P}}{\sigma_{PC}} + \frac{a_{i,W}}{\sigma_{PW}} \tag{4}$$

$$\frac{1}{\kappa_i} = \frac{a_{i,P}}{\kappa_{PC}} + \frac{a_{i,W}}{\kappa_{PW}} \tag{5}$$

$$\alpha_i = a_{i,P}\,\alpha_{PC} + a_{i,W}\,\alpha_{PW} \tag{6}$$

$$a_{i,P} + a_{i,W} = 1. \tag{7}$$

Here $\sigma_{PC(PW)}$, $\kappa_{PC(PW)}$ and $\alpha_{PC(PW)}$ are the conductivity, thermal conductivity and Seebeck coefficient of polycrystalline (powder) model of the sintered alloys, respectively and $i$ denotes $B$ (big) and $S$ (small).

Consider a simple two-band model [12,13] in which both bands have a parabolic energy-wave vector relationship with effective mass dependent on the temperature. In the two-band model, by considering an appropriate relaxation time, the thermal properties are given by

$$\sigma_{s,i} = \frac{2e^2\sqrt{2m_{s,i}}}{3\pi^2}\left(\frac{k_BT}{\hbar^2}\right)^{3/2} F_{i,3/2}(\eta_s^*) \tag{8}$$

$$\alpha_{s,i} = -\frac{k_B}{e}\left(\frac{F_{i,5/2}(\eta_s^*)}{F_{i,3/2}(\eta_s^*)} - \eta_s^*\right) \tag{9}$$

Here $m_{s,i=e(h)}$ denotes the effective mass of electrons (holes), and $s = (11, 33)$; $\eta_s^* \equiv \eta_s/k_BT$ is the reduced chemical potential (Fermi energy). $F_{i,n}$ represents an average relaxation time given by

$$F_{i,n} = \int \frac{\tau_{i,s} y^n e^{(y-\eta^*)}\,dy}{[1+e^{(y-\eta^*)}]^2} \tag{10}$$

where $\tau_{i,s}$ is the appropriate scattering rate. The Fermi energy is calculated numerically from the relation $n = 2\sum_k f_k$ [14]. The carrier distribution function $f_k$ is the Fermi function as follows:

$$f_k = \frac{1}{e^{(E(k)-\eta(n,T))/k_BT}+1}. \tag{11}$$

We have also considered the electron scattering processes with relaxation times caused by acoustic lattice vibrations and ionized impurities, using the following equation [15,16]:

$$\tau_{i,s}^{-1} = \tau_{L,i,s}^{-1} + \tau_{I,i,s}^{-1}. \tag{12}$$

The lattice contribution to the thermal conductivity is given by [17,18]

$$\kappa_{ph} = \frac{k_B}{2\pi^2 v_s}\left(\frac{k_B\theta}{\hbar}\right)^3\left(I_1 + \frac{I_2^2}{I_3}\right) \tag{13}$$

where

$$I_1 = \int_0^{\theta/T} \tau_{l,s}\frac{y^4e^y}{[e^y-1]^2}dy$$
$$I_2 = \beta\int_0^{\theta/T} \frac{\tau_{l,s}}{\tau_u}\frac{y^4e^y}{[e^y-1]^2}dy \tag{14}$$

$$I_3 = \beta\int_0^{\theta/T} \frac{1}{\tau_u}\left(1-\beta\frac{\tau_{l,s}}{\tau_u}\right)\frac{y^4e^y}{[e^y-1]^2}dy. \tag{15}$$

Here $\theta$ is the Debye temperature, and $v_s$ is the average velocity of sound. Under the assumption that the relaxation times for all scattering processes are independent,

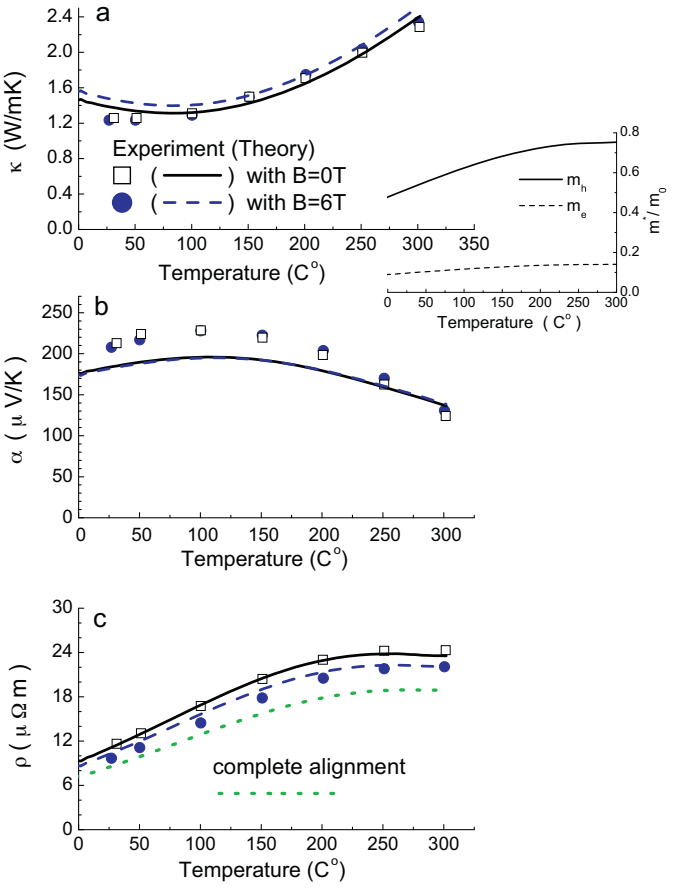


**Fig. 1.** (a) Thermal conductivities, (b) Seebeck coefficients and (c) resistivities of the $a$-axis direction of $Bi_{0.5}Sb_{1.5}Te_3$ alloys. Squares(circles) show the properties of the sintered alloy prepared in the absence of a magnetic field (in the presence of a $B = 6$ T magnetic field). Grains in the alloys had two sizes, 2/0.5 μm and 20/4 μm, in the $a$/$c$-axis directions, and the carrier concentration in the $a$-axis direction was $1.8 \times 10^{19}$ cm$^{-3}$. The dotted green line shows the theoretically calculated resistivity in a completely aligned alloy. (The insert shows the effective masses of the holes and electrons as a function of temperature.) (For interpretation of the references to color in this figure legend, the reader is referred to the web version of the article.)

the combined phonon scattering relaxation rate is given in the calculation of the lattice thermal conductivity by [17,18]

$$\tau_{l,s}^{-1} = (1+\beta)\tau_{u,s}^{-1} + \tau_{ph,s}^{-1} + \tau_{pd,s}^{-1} + \tau_{B,s}^{-1} \tag{16}$$

where $\tau_{u,s}^{-1}$ is the Umklapp three-phonon scattering rate, $\tau_{pd,s}^{-1}$ is the point defects-phonon scattering rate, $\tau_{ph,s}^{-1}$ is the electron–phonon scattering rate and $\tau_{B,s}^{-1}$ is the phonon-grain boundary scattering rate. The relaxation time $\tau_{B,s}$ for the phonon-grain boundary scattering is described by

$$\tau_{B,s} = \frac{l_g}{v_s} \tag{17}$$

where $l_g$ is the average grain-boundary size. This additional relaxation time gives rise to a decrease in the lattice thermal conductivity.

To investigate the thermal properties due to the additional carrier-grain boundary scattering, the relaxation time is described in the presence of grain boundaries:

$$\tau_g = \frac{l_g}{v} \tag{18}$$

where $v = [3k_BT/m^*]^{1/2}$ is the average thermal velocity [19]. The mobility due to the carrier-grain boundary scattering is given by the relaxation time $\tau_g$:

$$\mu_g = \frac{e\,\tau_g}{m^*} = \frac{e\,l_g}{\sqrt{3m^*k_BT}} \tag{19}$$

Therefore, the effective mobility $\mu_e$ is given by the grain boundary scattering

$$\frac{1}{\mu_e} = \frac{1}{\mu_0} + \frac{1}{\mu_g} \tag{20}$$

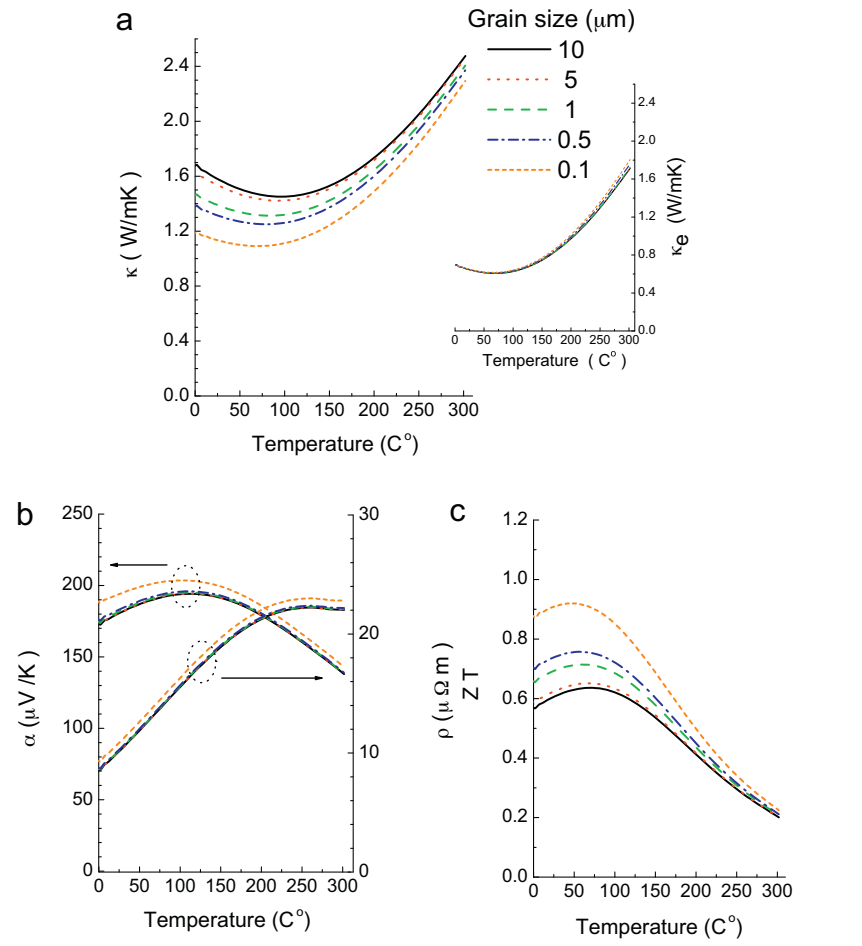


**Fig. 2.** (a) Theoretically calculated thermal conductivity, (b) Seebeck coefficient and resistivity and (c) the figure of merit (ZT) of the aligned p-type $Bi_{0.5}Sb_{1.5}Te_3$ alloys with one type of various round grain-sizes with diameters of 10, 5, 1, 0.5, 0.1 μm. (The insert shows the electronic thermal conductivities of the alloys.)

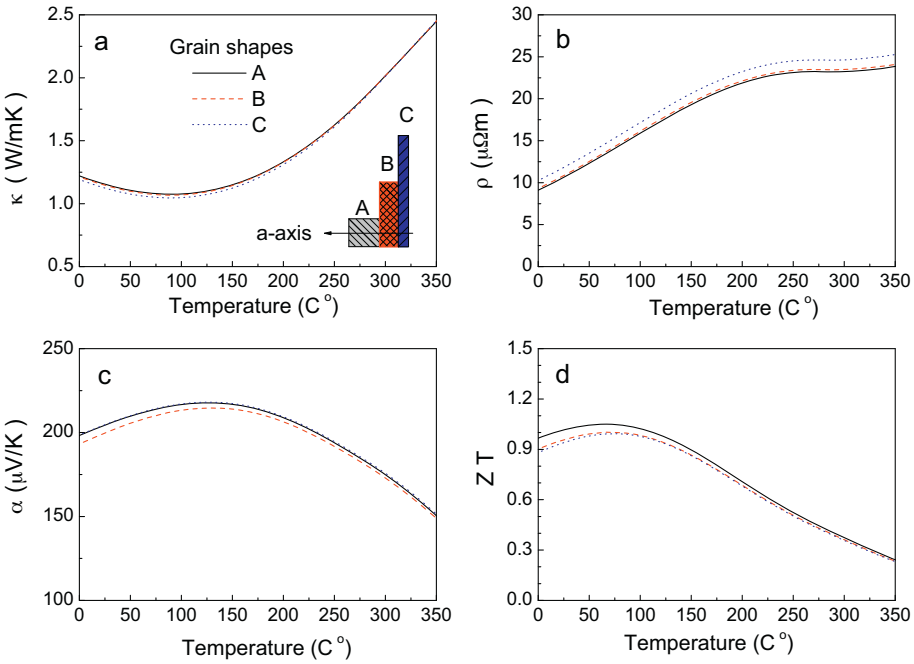


**Fig. 3.** (a) Theoretically calculated thermal conductivity, (b) resistivity, (c) Seebeck coefficient and (d) the figure of merit of the $Bi_{0.5}Sb_{1.5}Te_3$ alloys with three types of grain-shapes, all of which had the same volume, with $L_a < L_c$.

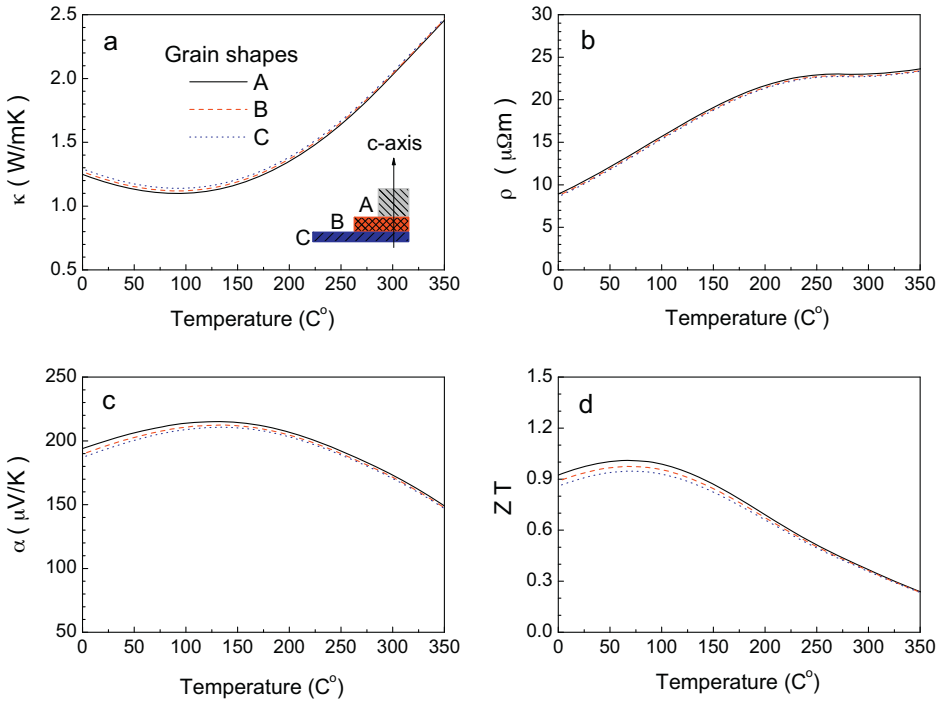


**Fig. 4.** (a) Theoretically calculated thermal conductivity, (b) resistivity, (c) Seebeck coefficient and (d) the figure of merit of the $Bi_{0.5}Sb_{1.5}Te_3$ alloys with three types of grain-shapes, all of which had the same volume, with $L_a > L_c$.

where $\mu_0$ is the mobility of the single crystal (alloy without grains). For the large grain size, the effective mobility should be the single crystal mobility, whereas for small grain size it will be limited by the grain boundary scattering. This effect may influence the thermal conductivity because of the Wiedemann–Franz ratio. Thus, the carrier part, $\kappa_{e,s}$, in the total thermal conductivity is determined using the Wiedemann–Franz ratio as $\kappa_{e,s} = L_s \sigma_s T$, where $L_s$ is the Lorentz number.

In addition, the band gap energy is also changed by the carrier confinement in the grain boundary

$$E_{gap} = E_0 + \frac{\hbar^2 \pi^2}{2m^* l_g^2} \tag{21}$$

where $E_0$ is the energy band gap of the single crystal. The effective mass is determined by the mobility and carrier concentration and depends on the temperature [20]. We assumed in the theoretical calculations that the complex band structure of anisotropic materials represents the two conduction-band model with a parabolic band structure and the changing effective mass for temperatures.

## 3. Results and discussion

The sintered $Bi_{0.5}Sb_{1.5}Te_3$ alloys have various grain types that can be classified into two types of randomization. One has grains with an average size of $L_a = 2.5\,\mu m$ (small particles) whose $c$-axes are completely randomly oriented in the medium, and the other has grains with an average size of $L_a = 20\,\mu m$ (big particles) whose $c$-axes are almost regularly oriented.

Fig. 1 shows the $\kappa$, $\alpha$, and $\rho$ values along the $a$-axis for the two types of prepared $Bi_{0.5}Sb_{1.5}Te_3$ alloys with a volume ratio of $V_{Big}/V_{Small} = 0.3/0.7$. The alloy prepared under the pure conditions (pure alloy) had $a_{B,P} = 0.5$ and $a_{S,P} = 0.27$ and the other prepared in the presence of a 6 T magnetic field (aligned alloy) had $a_{B,P} = 0.58$ and $a_{S,P} = 0.53$. The $c$-axes of the small grains in the alloy prepared in the presence of a magnetic field are more strongly aligned, 0.53 compared to 0.27. The grains in the alloys have two sizes, $L_a/L_c = 2.5/0.5\,\mu m$ and $L_a/L_c = 20/4\,\mu m$, and the carrier concentrations of the $a$-axis directions are about $1.8 \times 10^{19}\,cm^{-3}$ at room temperature and are almost unchanged until 100 °C. The using parameters in the model are obtained from the reported experimental results by the EBSD-SEM mapping analysis in Refs. [8,9]. We take the average grain sizes of $L_c = L_a/5$ along the $c$-axis. Experimental (calculated) results are denoted by open squares (dashed lines) for the pure alloy and open circles (solid lines) for the aligned alloy in Fig. 1. The experimental $\kappa$ values of both alloys are similar, as shown in Fig. 1(a). However, the calculated $\kappa$ value of the aligned alloy is higher than that in the pure alloy, because the $\kappa$ value of the $a$-axis is highly aligned in the 11-direction. The insert shows the effective masses of the holes and electrons in the alloys in the 11-direction. The product of the effective mass and mobility is one of the most important parameters effecting the thermoelectric efficiency in the extrinsic conduction region. The increase in the effective mass with temperature results from complex scattering mechanisms of carriers. The $\alpha$ value of both alloys are similar, as shown in Fig. 1(b). This result indicates that the Seebeck coefficient is almost unaffected by the crystalline alignment. Because the carrier concentrations of both directions does not changed due to the crystalline alignment. This result agrees with the theoretical results. Fig. 1(c) shows the $\rho$ value of the two alloys. The $\rho$ value of the aligned alloy has smaller than that of the pure alloy, because the aligned alloy has more aligned resistivities in the 11-direction. The dotted line shows the theoretical $\rho$ of the perfectly aligned alloy, that is, the polycrystalline phase of $Bi_{0.5}Sb_{1.5}Te_3$. Therefore, the thermoelectric efficiency is improved by the crystalline alignment of the $c$-axis in the grains. This improvement is mainly caused by the improved resistivity due to the enlarged alignment. The experimental results agree well with the theoretical calculations [9].

Fig. 2 shows the calculated thermoelectric properties of the aligned $Bi_{0.5}Sb_{1.5}Te_3$ alloys, in which the grains were all spherical with diameters of 10, 5, 1, 0.5, 0.1 μm. The decrease in $\kappa$ with decreasing grain size, as shown in Fig. 1(a), occurred because the phonon-grain scattering rates became dominant. The electronic thermal conductivity ($\kappa_e$) did not change for grain sizes over 0.1 μm, as shown in the insert. Therefore, we can see that thermal conductivity of the alloys with grain boundaries is determined almost exclusively by the phonon-grain boundary scattering. The $\alpha$ and $\rho$ values of the alloys with different grain sizes were constant up to 0.5 μm. The variations begin with under grain size of 0.1 μm. This variation is caused by the confinement of carriers in the grains,

the carrier-grain boundary scattering and change in the band gap energy. But, the hole-grain boundary scattering over grain size of 0.1 μm has little effect on the thermoelectric properties. Consequently, we found that the figure of merit of the alloy is improved with the small grain size, because of the phonon-grain boundary scattering.

Fig. 3 shows the calculated values of $\kappa$, $\alpha$, $\rho$ and figure of merit along the $a$-axis in the aligned $Bi_{0.5}Sb_{1.5}Te_3$ alloys with the three types of grain shapes ($L_a < L_c$), in which the same volumes are the same, $A = (0.1 \times 0.1) \times 0.1$, $B = (0.05 \times 0.05) \times 0.4$ and $C = (0.025 \times 0.025) \times 1.6\,(\mu m)^3$. In the case, we assume that their carrier concentrations are the same. These volumes were obtained by multiplying the grain area in the cleavage plane ($L_a \times L_a$) by the length ($L_c$) along the $c$-axis of the grains. The $\kappa$ with the small grain area becomes low, but it had a similar value for all samples, as shown in Fig. 3(a). It is caused by the phonon-grain boundary scattering. The $\rho$ value decreased as the grain volume became a cube, as shown in Fig. 3(b). It is caused by the reduced carrier-grain boundary scattering rate in the 11-direction. The $\alpha$ value for the strongly confined samples become large in the condition of the same carrier concentration. It is caused by the extended band gap due to the carrier confinement in the 11-direction. Consequently, we found that the figure of merit along the $a$-axis could be improved by making the grain shape more spherical.

Fig. 4 shows the calculated values of $\kappa$, $\alpha$, $\rho$ and figure of merit along the $a$-axis in the aligned $Bi_{0.5}Sb_{1.5}Te_3$ alloys with the three types of grain shapes ($L_a > L_c$), which have the same grain volumes, $A = (0.1 \times 0.1) \times 0.1$, $B = (0.14 \times 0.14) \times 0.05$ and $C = (0.2 \times 0.2) \times 0.025\,(\mu m)^3$. The grain areas in the cleavage plane increased as $L_c$ decreased. The $\kappa$ value decreased with stronger carrier confinement in the cleavage plane, as shown in Fig. 4(a). It will be more dominant in the higher aligned samples. The resistivities were almost the same. It results from the small carrier-grain boundary scattering in these sizes. The grain sizes of $L_c$ had no effect on the resistivity of the $a$-axis. The $\alpha$ values of the alloys are determined by the carrier confinement in the $c$-axis. In this case, the chemical potential energy was large, because the energy band gap is extended by the strong quantum confinement. Consequently, the figure of merit of sample A with more spherical grain areas increased.

## 4. Conclusion

The thermoelectric efficiency of $Bi_{0.5}Sb_{1.5}Te_3$ alloys was improved by increasing the crystalline alignment and by making the grains more spherical in the region of the same volume. This improvement mainly results from the improved thermal conductivity due to the phonon-grain boundary scattering and the band gap enhancement due to the more strong carrier confinement to the measuring direction.

## Acknowledgments

This research was supported by Basic Science Research Program through the National Research Foundation of Korea (NRF) funded by the Ministry of Education, Science and Technology (NRF-2010-0021173) and by Gyeongbuk Province and Gyeongju City through their support of the DGIST's Green Energy Research in the Republic of Korea.

## References

[1] M. Sttumorang, H.J. Goldsmid, Phys. Status Solidi B 134 (1986) 83.
[2] S. Pal, D.N. Bose, Solid State Commun. 97 (1996) 725.
[3] J.Y. Yang, T. Aizawa, A. Yamamoto, T. Ohta, J. Alloys Compd. 312 (2000) 326.
[4] C. Kim, D.H. Kim, Y.S. Han, J.S. Chung, H. Kim, J. Alloys Compd. 509 (2011) 609.
[5] Y. Xu, G. Xu, C. Ge, Scripta Mater. 58 (2008) 1070.
[6] H.J. Im, D.H. Kim, T. Mitani, K.C. Je, Jpn. J. Appl. Phys. 43 (2004) 1094.
[7] H.J. Im, D.H. Kim, J.S. Ahn, H. Iwasaki, S. Sano, K.C. Je, T. Mitani, Jpn. J. Appl. Phys. 43 (2004) 3548.
[8] D.H. Kim, C. Kim, S.H. Heo, H. Kim, Acta Mater. 59 (2011) 405.
[9] D.H. Kim, C. Kim, K.C. Je, G.H. Ha, H. Kim, Acta Mater. 59 (2011) 4957.
[10] D.H. Kim, C. Kim, D.W. Ha, H. Kim, J. Alloys Compd. 509 (2011) 5211.
[11] D.J. Ryden, J. Phys. C 4 (1971) 1193.
[12] C.B. Vining, J. Appl. Phys. 69 (1991) 331.
[13] R. Simom, J. Appl. Phys. 33 (1962) 1830.
[14] K.C. Je, K.C. Seo, Y. Kim, J. Appl. Phys. 86 (1999) 6196.
[15] W. Shpckley, J. Bardeen, Phys. Rev. 77 (1950) 388.
[16] V.I. Fistul, Heavily Doped Semiconductors, Plenum, New York, 1969.
[17] J. Callaway, Phys. Rev. 113 (1959) 1046.
[18] J. Callaway, H.C. von Bayer, Phys. Rev. 120 (1960) 1149.
[19] J.N. Roy, S. Basu, D.N. Bose, J. Appl. Phys. 54 (1983) 847.
[20] V.A. Kutasov, L.N. Luk'yanova, P.P. Konstantinov, G.T. Alekseeva, Phys. Solid State 39 (1997) 419.